

# Learning Energy-Based Models With Adversarial Training

Xuwan Yin<sup>✉</sup>, Shiyang Li<sup>✉</sup>, and Gustavo K. Rohde<sup>✉</sup>

University of Virginia  
{xy4cm, sl8jx, gustavo}@virginia.edu

**Abstract.** We study a new approach to learning energy-based models (EBMs) based on adversarial training (AT). We show that (binary) AT learns a special kind of energy function that models the support of the data distribution, and the learning process is closely related to MCMC-based maximum likelihood learning of EBMs. We further propose improved techniques for generative modeling with AT, and demonstrate that this new approach is capable of generating diverse and realistic images. Aside from having competitive image generation performance to explicit EBMs, the studied approach is stable to train, is well-suited for image translation tasks, and exhibits strong out-of-distribution adversarial robustness. Our results demonstrate the viability of the AT approach to generative modeling, suggesting that AT is a competitive alternative approach to learning EBMs.

**Keywords:** Adversarial Training, Adversarial Attacks, Energy-Based Models (EBMs), Generative Modeling

## 1 Introduction

In unsupervised learning, energy-based models (EBMs) [37] are a class of generative model that uses an energy function to model the probability distribution of the observed data. Unlike explicit density models, EBMs model the unnormalized density function, which makes it difficult to evaluate the likelihood function. Maximum likelihood learning of EBMs hence makes use of the likelihood function’s gradient which can be approximated using Monte Carlo methods. Each iteration of the learning process involves first generating synthesized data by sampling from the current model, and then updating the model to maximize the energy difference between synthesized data and observed data. This process leads to an energy function that outputs low energies on the data manifold and high energies on other regions. EBMs find applications in image restoration (denoising, inpainting, etc), out-of-distribution detection, and various sample generation tasks. The main difficulties of training EBMs lie in the computational challenges from the sampling procedure and some training stability issues [12,44,43,16,17,11,71,61].

Another line of work on adversarial training (AT) show that adversarially robust classifiers learn high-level, interpretable features, and can be utilized to solve

various computer vision tasks including generation, inpainting, super-resolution, and image-to-image translation [57,28,13,51]. Compared to state-of-the-art generative models, this AT approach does not provide a competitive generation performance and is therefore of limited value in many of these tasks. Nonetheless, the generative properties of the robust classifier suggest that the model has captured the distribution of the training data, although the underlying learning mechanism is not yet well understood.

At a high level, both EBMs training and AT are based on the idea of first using gradient-based optimization to generate samples that reach high activation under the current model, and then optimizing the model to minimize its activation on the generated samples. In addition, both approaches synthesize new samples by performing gradient descent on the trained model. These similarities suggest that there are some connections between these two approaches.

In this work we investigate the mechanism by which AT learns data distributions, and propose improved techniques for generative modeling with AT. We focus on binary AT [69] which does not require class labels and hence naturally fits the generative modeling task. We first analyze the binary AT objective and the corresponding training algorithm, and show that binary AT learns a special kind of energy function that models the support of the observed data. We then draw a connection between AT and MCMC-base maximum likelihood learning of EBMs by showing that the binary AT objective can be interpreted as a gradient-scaled version of the likelihood objective in EBMs training, and the PGD attack can be viewed as a non-convergent sampler of the model distribution. This connection provides us with intuition of how AT learns data distributions from a maximum likelihood learning perspective, and suggests that binary AT can be viewed as an approximate maximum likelihood learning algorithm.

We further propose improved techniques for generative modeling with AT based on the above analysis. Our empirical evaluation shows that this AT approach provides competitive generation performance to explicit EBMs, and at the same time is stable to train (just like regular adversarial training), is well-suited for image translation tasks, and exhibits strong out-of-distribution adversarial robustness. The main limitation of the studied approach is that it cannot properly learn the underlying density function of the observed data. However, this problem is not unique to the studied approach - most existing work on learning EBMs relies on short-run non-convergent sampler to improve the training efficiency, and the learned model typically does not have a valid steady-state that reflects the distribution of the observed data [44,43].

In summary, the contributions of this paper are: 1) We show that binary AT learns a special kind of energy function that models the support of the data distribution, and the learning process is closely related to MCMC-based maximum likelihood learning of EBMs. 2) We propose improved techniques for generative modeling with AT, and demonstrate competitive image generation performance to state-of-the-art explicit EBMs. 3) We show that the studied approach is stable to train, has competitive training and test time sampling

efficiency, and can be applied to denoising, inpainting, image translation, and worst-case out-of-distribution detection.

## 2 Related Work

**Learning EBMs.** Due to the intractability of the normalizing constant in the EBMs likelihood function, maximum likelihood learning of EBMs makes use of the gradient of the log-likelihood which can be approximated using MCMC sampling. Recent work [63,12,44,43] scaling EBMs training to high-dimensional data performs sampling using SGLD [60] and initialize the chain from a noise distribution. The sampling process involves estimating the model’s gradient with respect to the current sample at each step and therefore has high computational cost. To improve the sampling efficiency, many authors consider short-run non-convergent SGLD sampler in combination with a persistent sampling buffer [12,43,16,17,61,11]. Although a short-run sampler is sufficient for learning a generation model, the resulting energy function typically does not have a valid steady-state [44,43]. The mixing time of the sampling procedure also depends on how close the chain-initialization distribution is to the model distribution. A recent trend hence considers initializing the sampling chain from samples produced by a generator fitted on the target distribution [62,35,20,45,21,17,61,67,1,42,68].

Maximum likelihood learning of EBMs also has some training stability issues, and various techniques have been developed to address these issues. These techniques include 1) using weight normalization [50], Swish activation [47], gradient clipping, and weight decay (see [61]), 2) gradient norm clipping on model parameters and using a KL term in the training objective (see [11]), 3) adjusting learning rate and SGLD steps during training and adding Gaussian noise to input images (see [16]), 4) gradient clipping on SGLD and model parameters and spectral normalization (see [12]), and 5) multiscale training and smooth activation functions (see [71]). Overall, there does not seem to have a consensus on how to stabilize EBMs training. Due to the computational challenge of MCMC sampling and stability issues, the successful application of EBMs to modeling high-dimensional data such as  $256 \times 256$  images is only achieved in some very recent works [61,71].

Aside from MCMC-based maximum likelihood learning of EBMs, alternative approaches for learning EBMs exist. Score matching [27] circumvents the difficulty of estimating the partition function by directly modeling the derivatives of the data distribution. Score matching has recently been successfully applied to modeling large natural images and achieves competitive performance to state-of-the-art generative models such as GANs [53,54,55,26]. Noise contrastive estimation (NCE) [19] learns data distributions by contrasting the observed data with data from a known noise distribution. Similar to our approach, NCE makes use of a logistic regression model. The main difference is that in NCE, the logit of the classifier is the difference in log probabilities of the model distribution and the noise distribution, whereas in our approach the logit directly defines the

estimator (i.e., the energy function). Unlike other EBMs, NCE typically does not scale well to high-dimensional data [19,5,48].

**Maximin interpretation of EBMs.** When the noise term in the SGLD sampler is disabled, the learning process of EBMs can be interpreted as solving a *maximin* game [65,66,64]. This interpretation coincides with our formulation in Eq. (5). The key differences lie in the value function, the setting of the sampler (SGLD vs. PGD attack), and the Markov chain initiation distribution.

**Understanding and Improving AT Generative Model.** Our work is related to [73,59] which are also attempts to understand and improve AT’s generative capability. [73,59]’ focus is on the *supervised setting*, where they use the concept of learning class-conditional energy functions to understand adversarially robust classifiers’ generative capability. Our analysis is in an *unsupervised setting*, where we attempt to understand *binary* AT’s generative property by connecting it with the standard EBMs formulation (Eq. (1)). Although [59] also considers the unsupervised scenario, their unsupervised generative model is a contrastive learning model [30] which requires training samples to perform test-time sampling. Our generative model is based on binary AT and follows the standard practice of MCMC sampling from the learned energy function. In addition to the theoretical analysis, we propose improve training techniques that allow us to obtain a significantly better FID on CIFAR-10 (Tab. 2) and successfully scale the training to  $256 \times 256$  datasets.

### 3 Background

#### 3.1 Energy-Based Models

Energy-based models (EBMs) [37] represent probability distributions by converting the outputs of a scalar function  $f_\theta$  into probabilities through a Gibbs distribution:

$$p_\theta(x) = \frac{\exp(f_\theta(x))}{Z(\theta)}, \quad (1)$$

where the normalizing constant  $Z(\theta)$ , also known as the partition function, is an integral over the unnormalized probability of all states:  $Z(\theta) = \int \exp(f_\theta(x)) dx$ . The energy function is defined as  $E_\theta(x) = -f_\theta(x)$ , and thus has the property of attributing low energy outputs on the support of the target data distribution and high energy outputs in other regions.

For many interesting models, the partition function  $Z(\theta)$  is intractable, and therefore maximum likelihood estimation (MLE) of the model parameters  $\theta$  is not directly applicable. Standard maximum likelihood learning of EBMs makes use of the gradient of the log likelihood function. Denote the distribution of the observed data as  $p_{\text{data}}$ , the gradient of the log likelihood takes the form

$$\nabla_\theta \mathbb{E}_{x \sim p_{\text{data}}} [\log p_\theta(x)] = \mathbb{E}_{x \sim p_{\text{data}}} [\nabla_\theta f_\theta(x)] - \mathbb{E}_{x \sim p_\theta(x)} [\nabla_\theta f_\theta(x)]. \quad (2)$$



Intuitively, maximizing log-likelihood with this gradient causes  $f_\theta(x)$  to increase on  $p_{\text{data}}$  samples and decrease on samples drawn from  $p_\theta$ ; when  $p_\theta$  matches  $p_{\text{data}}$ , the gradient cancels out and the training terminates.

Evaluating  $\mathbb{E}_{x \sim p_\theta(x)} \nabla_\theta f_\theta(x)$  requires sampling from the model distribution. This can be done with Markov chain Monte Carlo (MCMC) methods. Recent work scaling EBMs training to high-dimensional data [63,12,44,43] makes use of the SGLD method [60] which samples the model distribution by

$$x_0 \sim p_0, \quad x_{i+1} = x_i + \frac{\lambda}{2} \nabla_x f_\theta(x_i) + \epsilon, \quad \epsilon \sim \mathcal{N}(0, \lambda), \quad (3)$$

where  $p_0$  is some random noise distribution. A proper SGLD sampler requires a large number of update steps in order for the distribution of sampled data to match  $p_\theta$ . Due to the high computational cost of this sampling process, many authors resort to short-run non-convergent MCMC to improve the sampling efficiency[44,43,12,63,16]. The resulting model typically does not have a valid steady-state that reflects the distribution of the observed data, but is still capable of generating realistic and diverse samples [44,43].

### 3.2 Binary Adversarial Training

Binary adversarial training [69] is a method for detecting adversarial examples. In a  $K$  class classification problem, the detection method consists of  $K$  binary classifiers, with the  $k$ -th binary classifier trained to distinguish clean data of class  $k$  from adversarially perturbed data of other classes. A committee of  $K$  binary classifiers then provides a complete solution for detecting adversarially perturbed samples of any classes.

Denote the data distribution of class  $k$  as  $p_{\text{data}}$ , the mixture distribution of other classes as  $p_0 = \frac{1}{K-1} \sum_{i=1, \dots, K, i \neq k} p_i$ , the  $k$ -th binary classifier is trained by maximizing the objective

$$J(D) = \mathbb{E}_{x \sim p_{\text{data}}} [\log D(x)] + \mathbb{E}_{x \sim p_0} [\min_{x' \in \mathbb{B}(x, \epsilon)} \log(1 - D(x'))], \quad (4)$$

where  $D : \mathcal{X} \subseteq \mathbb{R}^d \rightarrow [0, 1]$  is the classification function, and  $\mathbb{B}(x, \epsilon)$  is a neighborhood of  $x$ :  $\mathbb{B}(x, \epsilon) = \{x' \in \mathcal{X} : \|x' - x\|_2 \leq \epsilon\}$ . In practice,  $D$  is defined by applying a logistic sigmoid function to the output of a neural network:

$$D(x) = \sigma(f_\theta(x)), \quad (5)$$

where  $f_\theta$  is a neural network with a single output node and parameters  $\theta$ .

The inner minimization in Eq. (4) is solved using the PGD attack [38,36], a first-order method that employs an iterative update rule of ( $l^2$ -based attack):

$$x_0 \sim p_0, \quad x_{i+1} = \text{Proj}(x_i - \lambda \frac{\nabla_x \log(1 - D(x_i))}{\|\nabla_x \log(1 - D(x_i))\|_2}), \quad (6)$$

where  $\lambda$  is some step size, and Proj is the operation of projecting onto the feasible set  $\mathbb{B}(x, \epsilon)$ . Because the gradient vector in Eq. (6) is normalized to have

unit norm, we can equivalently implement the attack by directly performing gradient ascent on  $f_\theta$ :

$$x_0 \sim p_0, \quad x_{i+1} = \text{Proj}\left(x_i + \lambda \frac{\nabla_x f_\theta(x_i)}{\|\nabla_x f_\theta(x_i)\|_2}\right). \quad (7)$$

## 4 Binary AT Generative Model

In this section we develop a generative model based on binary AT. We first analyze the optimal solution to the binary AT problem, and then investigate the mechanism by which binary AT learns the data distribution, and finally interpret the learning process from the maximum likelihood learning perspective. Our main result is that under a proper configuration of perturbation limit and  $p_0$  data, binary AT learns a special kind of energy function that models the support of  $p_{\text{data}}$ . Based on these theoretical insights, we proposed improved training techniques.

### 4.1 Optimal Solution to the Binary AT Problem

We consider the optimal solution of Eq. (4) under the scenario of unbounded perturbation:  $\mathbb{B}(x, \epsilon) = \mathcal{X}$ . This allows us to further simplify the PGD attack by removing the Proj operator:

$$x_0 \sim p_0, \quad x_{i+1} = x_i + \lambda \frac{\nabla_x f_\theta(x_i)}{\|\nabla_x f_\theta(x_i)\|_2}. \quad (8)$$

Perturbing  $p_0$  samples can be thought of as moving  $p_0$  samples via a translation function  $T(x) = x + \Delta_x$ , with  $\Delta_x$  being the perturbation computed on sample  $x$ . We can write the density function of the perturbed distribution  $p_T$  using random variable transformation:

$$p_T(z) = \int_{\mathcal{X}} p_0(x) \delta(z - T(x)) dx. \quad (9)$$

The inner problem in Eq. (4) can then be interpreted as determining the distribution which has the lowest expected value of  $\log(1 - D(x))$ :

$$p_T^* = \arg \min_{p_T} \mathbb{E}_{x \sim p_T} [\log(1 - D(x))]. \quad (10)$$

The objective of the outer problem is then the log-likelihood in a logistic regression model which discriminates  $p_{\text{data}}$  samples from  $p_T^*$  samples:

$$J(D) = \mathbb{E}_{x \sim p_{\text{data}}} [\log D(x)] + \mathbb{E}_{x \sim p_T^*} [\log(1 - D(x))]. \quad (11)$$

We can equivalently formulate Eq. (4) as a *maximin* problem

$$\max_D \min_{p_T} U(D, p_T) = \mathbb{E}_{x \sim p_{\text{data}}} [\log D(x)] + \mathbb{E}_{x \sim p_T} [\log(1 - D(x))], \quad (12)$$

and obtain its optimal solution by following the standard approach to solving maximin problems:

**Proposition 1.** *The optimal solution of  $\max_D \min_{p_T} U(D, p_T)$  is  $U(D^*, p_T^*) = -\log(4)$ , where  $D^*$  outputs  $\frac{1}{2}$  on  $\text{Supp}(p_{\text{data}})$  and  $\leq \frac{1}{2}$  outside  $\text{Supp}(p_{\text{data}})$ , and  $p_T^*$  is supported in the contour set  $\{D = \frac{1}{2}\}$ .*

*Proof.* See the supplementary materials.

The above maximin problem can also be interpreted as a two-player zero-sum game, and is closely related to GANs [15]’s *minimax* game which has the form

$$\min_G \max_D V(D, G) = \mathbb{E}_{x \sim p_{\text{data}}} [\log D(x)] + \mathbb{E}_{z \sim p_z} [\log(1 - D(G(z)))]. \quad (13)$$

The game-theory point of view provides a convenient way to understand their differences. We include a game theory-based analysis of  $\max_D \min_{p_T} U(D, p_T)$  and a comparative analysis of GANs in the supplementary materials.

## 4.2 Learning Mechanism

Proposition 1 states that by solving  $\max_D \min_{p_T} U(D, p_T)$  we can obtain a  $D$  that outputs  $\frac{1}{2}$  on the support of  $p_{\text{data}}$  and  $\leq \frac{1}{2}$  on other regions. This result is obtained by assuming that for any  $D$ , the inner minimization Eq. (10) is always perfectly solved. In practice, when  $D$  is randomly initialized, it has many local maxima outside the support of  $p_{\text{data}}$ . Because the inner minimization is solved by taking  $p_0$  samples and then performing gradient ascent on  $D$  with Eq. (8), this process can get trapped in different local maxima of  $D$ . Hence we can think of this process as searching for these local maxima and then put the perturbed  $p_0$  data in these regions. Then in the model update stage (outer maximization),  $D$  is updated by increasing its outputs on  $p_{\text{data}}$  samples and decreasing its outputs on the perturbed  $p_0$  data. By repeating this process, local maxima get suppressed and the model learns to correctly model  $\text{Supp}(p_{\text{data}})$ .

The algorithm for solving the maximin problem is described in Algorithm 1. Fig. 1 left panel shows the 2D simulation result of the algorithm when the  $p_0$  dataset contains random samples from the uniform distribution. It can be seen that when the algorithm converges, local maxima outside  $\text{Supp}(p_{\text{data}})$  are suppressed, and  $D$  (approximately) outputs  $\frac{1}{2}$  on  $\text{Supp}(p_{\text{data}})$  as predicted by Proposition 1. Meanwhile,  $D$  retains the gradient information for translating out-distribution samples to  $\text{Supp}(p_{\text{data}})$ .

Because the PGD attack is deterministic gradient ascent, its ability to discover different local maxima depends on the diversity of  $p_0$  samples. Fig. 1 right panel shows that when  $p_0$  data is concentrated in the bottom left corner, the final  $D$  still has local maxima outside the support of  $p_{\text{data}}$ . These local maxima are not suppressed because they were never discovered by the perturbed  $p_0$  data.

The above analysis reveals how binary AT learns data distributions: *the learning starts with a randomly-initialized  $D$  solution, and then iteratively refine the solution by suppressing local maxima outside the support of the target distribution.* This process is similar to EBMs training where the model distribution’s spurious modes are constantly discovered by MCMC sampling and subsequently

suppressed in the model update stage. However, unlike the EBMs likelihood objective Eq. (2), the AT objective Eq. (5) cannot properly learn the density function, but can only capture its support. This is corroborated by the 2D experiment where  $D$  outputs  $\frac{1}{2}$  uniformly on the support of  $p_{\text{data}}$  (blue points).

---

**Algorithm 1** Binary Adversarial Training

---

- 1: **repeat**
  - 2:   Draw samples  $\{x_i\}_{i=1}^m$  from  $p_{\text{data}}$ , and samples  $\{x_i^0\}_{i=1}^m$  from  $p_0$ .
  - 3:   Update  $\{x_i^0\}_{i=1}^m$  by performing  $K$  steps PGD attack Eq. (8) on each sample. Denote the resulting samples as  $\{x_i^*\}_{i=1}^m$ .
  - 4:   Update  $D$  by maximizing  $\frac{1}{m} \sum_{i=1}^m \log D(x_i) + \frac{1}{m} \sum_{i=1}^m \log(1 - D(x_i^*))$  (single step).
  - 5: **until**  $D$  convergences
- 

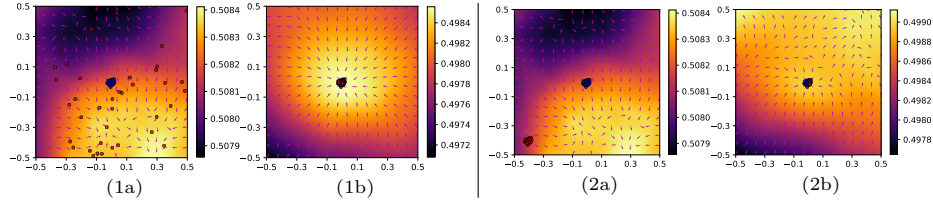


**Fig. 1.** Plots of contours and (normalized) gradient vector fields of the  $D$  functions learned with different  $p_0$  data. Left and right panel respectively show the initial state (1a and 2a) and final state (1b and 2b) of  $D$  when  $p_0$  data is respectively uniformly distributed (red points in 1a) and concentrated in the lower left corner (red points in 2a).  $p_{\text{data}}$  is a Gaussian distribution centered at  $(0, 0)$  (blue points).

### 4.3 Maximum Likelihood Learning Interpretation

We next consider the learning process of binary AT from a maximum likelihood learning point of view. Both binary AT and MCMC-based EBMs learning employ an iterative optimization algorithm, where in each iteration the contrastive data is computed by performing gradient ascent on the current model, and then the model is updated by maximizing its outputs on the observed data and minimizing its outputs on the contrastive data. The following analysis shows that the PGD attack can be viewed as a non-convergent sampler of the model distribution, and the binary AT objective Eq. (11) can be interpreted as a gradient-scaled version of the EBMs objective Eq. (2). Tab. 1 summarizes their key differences.

**Contrastive Data Computation.** In EBMs training, the contrastive data is computed by MCMC-sampling, typically with Langevin dynamics Eq. (3). In binary AT, the contrastive data is computed using the PGD attack Eq. (8).

**Table 1.** Key differences between binary AT and maximum likelihood EBMs.

<b>Objective gradient</b>	EBMs: $\mathbb{E}_{x \sim p_{\text{data}}}[\nabla_{\theta} f_{\theta}(x)] - \mathbb{E}_{x \sim p_{\theta}(x)}[\nabla_{\theta} f_{\theta}(x)]$
	Binary AT: $\mathbb{E}_{x \sim p_{\text{data}}}[(1 - \sigma(f_{\theta}(x)))\nabla_{\theta} f_{\theta}(x)] - \mathbb{E}_{x \sim p_T^*}[\sigma(f_{\theta}(x))\nabla_{\theta} f_{\theta}(x)]$
<b>Contrastive data</b>	EBMs: $x_0 \sim p_0, x_{i+1} = x_i + \frac{\lambda}{2}\nabla_x f_{\theta}(x_i) + \epsilon, \epsilon \sim \mathcal{N}(0, \lambda)$
	Binary AT: $x_0 \sim p_0, x_{i+1} = x_i + \lambda \frac{\nabla_x f_{\theta}(x_i)}{\ \nabla_x f_{\theta}(x_i)\ _2}$
<b><math>p_0</math> data</b>	EBMs: A noise distribution or a distribution close to $p_{\text{data}}$
	Binary AT: A real and diverse out-distribution dataset (80 million tiny images for CIFAR-10 and ImageNet for 256x256 datasets).

Comparing Eq. (8) with Eq. (3), we find that both approaches compute the contrastive data by first initializing from some out-distribution data, and then performing gradient ascent on  $f_{\theta}$ . The main differences are that the PGD attack does not have the noise term, and makes use of normalized gradient. Intuitively, the noise term enables the sampler to explore different modes by helping gradient ascent escape local maxima. Although the PGD attack does not have the noise term, its ability to explore different modes can be enhanced by using a diverse  $p_0$  dataset (Fig. 3).

In the PGD attack, as the normalized gradient vector has unit norm, the perturbation imposed on  $x_i$  is  $\lambda$ ; in a  $K$  iterations of the update, the overall perturbation  $\|x_i^* - x_i\|_2$  is always  $\leq \lambda K$ . Hence with the PGD attack we can more easily control the distribution of the contrastive data. In contrast, Langevin dynamics adjusts  $x_i$  in a scale that corresponds to the magnitude of the gradient of  $f_{\theta}$  at  $x_i$ ; when  $f_{\theta}$  is updated during training, the overall perturbation may undergo a large change. This behavior of Langevin dynamics can be a source of some training stability issues [43].

**Gradient of the Training Objective.** By definition Eq. (5), the gradient of  $D$ 's training objective Eq. (11) takes the form

$$\nabla_{\theta} J(D) = \mathbb{E}_{x \sim p_{\text{data}}}[(1 - \sigma(f_{\theta}(x)))\nabla_{\theta} f_{\theta}(x)] - \mathbb{E}_{x \sim p_T^*}[\sigma(f_{\theta}(x))\nabla_{\theta} f_{\theta}(x)]. \quad (14)$$

Comparing the above equation with Eq. (2) we find both equations consisting of gradient terms that yield similar effects: the first term causes  $f_{\theta}$  outputs on  $p_{\text{data}}$  samples to increase, and the second causes  $f_{\theta}$  outputs on the contrastive samples to decrease. Specifically, as  $(1 - \sigma(f_{\theta}(x)))$  and  $\sigma(f_{\theta}(x))$  are scalars in the range 0 to 1, the two gradient terms in Eq. (14) are respectively the scaled versions of the gradient terms in Eq. (2). It should be noted that although these scalars do not change the gradient update direction of individual terms in the model parameter space, the overall gradient update directions of Eq. (14) and Eq. (2) can be different.

Eq. (14) also helps to understand why binary AT can only learn the support of the observed data. In Eq. (2), when  $p_{\theta}(x)$  matches  $p_{\text{data}}$ , the gradient cancels out and training terminates, whereas in Eq. (14), when  $p_T^*$  matches  $p_{\text{data}}$  the gradient becomes  $\mathbb{E}_{x \sim p_{\text{data}}}[(1 - 2\sigma(f_{\theta}(x)))\nabla_{\theta} f_{\theta}(x)]$  and only vanishes when  $\sigma(f_{\theta}(x)) = \frac{1}{2}$

everywhere on the support of  $p_{\text{data}}$ . This result is consistent with Proposition 1 and the 2D experiment result.

#### 4.4 Improved Training of Binary AT Generative Model

**Diverse  $p_0$  Data.** As discussed in Sec. 4.2, a diverse  $p_0$  dataset improve the PGD attack’s ability to explore different local maxima of  $D$ . To validate this 2D intuition generalizes to high dimensions, we evaluate the image generation performances of models trained with different  $p_0$  datasets. Fig. 3 shows that the best FID is obtained when  $p_0$  is the most diverse dataset among the considered  $p_0$  datasets. (Note that we have used the same setting of the PGD attack and source images dataset to perform test-time generation in these three experiments.)

We follow existing work on adversarial training and use a  $p_0$  dataset that contains real data samples to train the model. Using a real dataset (as opposed to a noise distribution) helps the model achieve out-of-distribution adversarial robustness (Sec. 5.2 OOD detection) and learn informative gradient for transforming real out-distribution samples (not just noise samples) into valid samples of  $p_{\text{data}}$ . The latter can be a useful feature in image translation applications (Sec. 5.2). The setting of  $p_0$  in our experiments can be found in Tab. 1.

**Training With Unconstrained Perturbations.** Existing work on using adversarial training to train robust classifiers uses a small, fixed perturbation limit [38]. In the generative modeling task, we would like the perturbed  $p_0$  data to travel in a larger space to find more local maxima. This can be achieved by taking more PGD attack steps ( $K$ ) in step 3 of Algorithm 1. Fig. 4 shows that a larger  $K$  results in better FID scores.

The downside of a large  $K$  is that it converges slower because more gradient steps are taken in each iteration (Fig. 5  $K = 25$  vs.  $K = 5$ ). To improve the training efficiency we propose a mixed scenario in which we progressively increase the  $K$  value during training. We observe that this progressive training scenario converges faster than training with fixed- $K$  (Fig. 5  $K = 0, 1, \dots, 25$  vs.  $K = 25$ ). The pseudo code for progressive training is in Algorithm 2.

---

#### Algorithm 2 Progressive Binary Adversarial Training

---

```

1: for  $K$  in  $[0, 1, \dots, N]$  do
2:   for number of training iterations do
3:     Draw samples  $\{x_i\}_{i=1}^m$  from  $p_{\text{data}}$ , and samples  $\{x_i^0\}_{i=1}^m$  from  $p_0$ .
4:     Update  $\{x_i^0\}_{i=1}^m$  by performing  $K$  steps unconstrained PGD attack Eq. (8) on
       each sample. Denote the resulting samples as  $\{x_i^*\}_{i=1}^m$ .
5:     Update  $D$  by maximizing  $\frac{1}{m} \sum_{i=1}^m \log D(x_i) + \frac{1}{m} \sum_{i=1}^m \log(1 - D(x_i^*))$ .
6:   end for
7: end for

```

---

**Regularization.** While other generative models typically require some forms of regularization, the proposed model can be trained successfully without using any regularization. One trick that we find beneficial for achieving better FID (Fig. 2,  $R_1$  reg = 30, pretrained vs. from scratch) is to pretrain the  $D$  model on the ImageNet classification task. (This requires adding auxiliary output nodes which are ignored when later training the  $D$  model.) When using the pretrained model, we find it necessary to use  $R_1$  regularization [40], otherwise the FID stops improving after a few hundred iterations (Fig. 2,  $R_1$  reg = 0 pretrained). Note that when  $D$  is trained from scratch,  $R_1$  regularization is not strictly required, but adding the regularizer does not hurt the performance (Fig. 2,  $R_1$  reg = 0 from scratch vs.  $R_1$  reg = 30 from scratch).

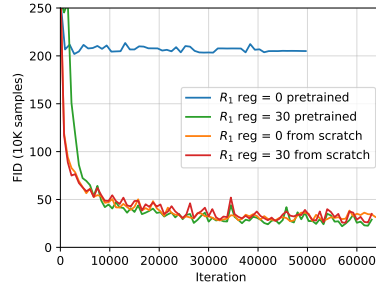


**Fig. 2.** The effect of  $R_1$  regularization on CelebA-HQ.

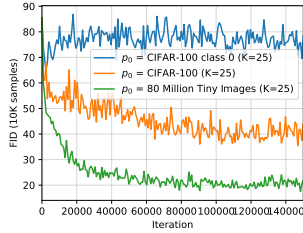


**Fig. 3.** FID scores obtained with models trained with different  $p_0$ s on CIFAR-10.

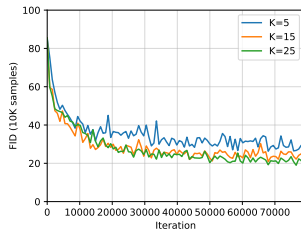


**Fig. 4.** FID scores obtained with different  $K$ s in Algorithm 1 on CIFAR-10.

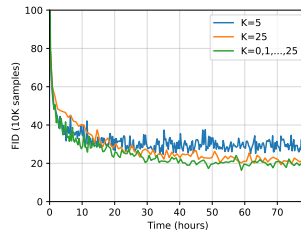


**Fig. 5.** Progressive training vs. training with fixed- $K$  on CIFAR-10.

## 5 Experiments

In this section we provide an empirical evaluation of the proposed AT generative model. We first evaluate the approach’s image generation performance and then demonstrate its applications to image-to-image translation and worst-case out-of-distribution detection. We further provide an analysis of the proposed approach’s training stability in Sec. 5.3.

In the supplementary materials we provide experiment setup details including model architectures, training hyperparameters, sample generation settings, and evaluation protocols. We also include additional results including sampling efficiency analysis, uncured image generation and image translation results, and demonstration of applications to denoising, inpainting, and compositional visual generation [10]. The interpolation results and nearest neighbor analysis in the



supplementary materials suggest that our model captures the manifold structure of the observed data, as opposed to simply memorizes the data samples.

### 5.1 Image Generation

Tab. 2 shows that on CIFAR-10 [34] our approach achieves the best Inception Score (IS) [49] and FID [25] among AT generative models. Our approach also improves over state-of-the-art explicit EBMs in terms of IS, and at the same time has a slightly worse FID. Compared to VAEBM [61], our method does not require an auxiliary model to train, and has better test time sampling efficiency (see supplementary materials). Diffusion Recovery [14] trains a sequence of conditional EBMs, with each one defining the conditional distribution of a noisy sample given the same sample at a higher noise level. Similar to score-based approaches, these conditional EBMs do not directly model the data distribution of the observed data, so it is unclear how these models can be applied to tasks which require explicit knowledge of the data distribution (e.g., OOD detection).

Tab. 3 shows that on CelebA-HQ 256 [31] our method outperforms or is on par with state-of-the-art generative models except GANs. On LSUN Church [70] our method outperforms a latest energy-based model VAEBM [61] (the authors only provided the  $64 \times 64$  result), but falls below DDPM and GANs. Fig. 6 shows sample image generation results.

**Table 2.** IS and FID scores on CIFAR-10

	Approach	IS $\uparrow$	FID $\downarrow$
AT-based	Ours	9.10	13.21
	CEM [59]	8.68	36.4
	JEAT [73]	8.80	38.2
	Adv. Robust Classifier [51]	7.5	-
Explicit EBMs	Diffusion Recovery [14]	8.30	9.58
	VAEBM [61]	8.43	12.19
	CoopFlow [68]	-	15.80
	CF-EBM [71]	-	16.71
	ImprovedCD [11]	7.85	25.1
	VERA [17]	-	27.5
	EBMs-VAE [67]	6.65	36.2
	JEM [16]	8.76	38.4
	IGEBM (Ensemble) [12]	6.78	38.2
GANs	Short-Run EBMs [44]	6.21	44.16
	StyleGAN2 w/o ADA [32]	8.99	9.9
	BigGAN [4]	9.22	14.73
	SNGAN [41]	8.22	21.7
	WGAN-GP [18]	7.86	36.4
Score-based	SDE [55]	9.89	2.20
	DDPM [26]	9.46	3.17
	NCSNv2 [54]	8.4	10.87
	NCSN [53]	8.87	25.32

**Table 3.** FID scores on CelebA-HQ 256, AFHQ-CAT [6], and LSUN Church 256

Dataset	Approach	FID $\downarrow$
CelebA-HQ 256	Ours	17.31
	VAEBM [61]	20.38
	CF-EBM [71] ( $128 \times 128$ )	23.50
	NVAE [58]	45.11
	GLOW [33]	68.93
	Adversarial Latent AE [46]	19.21
	ProgressiveGAN [31]	8.03
AFHQ-CAT	Our ( $256 \times 256$ )	13.35
	StyleGAN2 ( $512 \times 512$ ) [32]	5.13
LSUN Church	VAEBM ( $64 \times 64$ ) [61]	13.51
	Ours ( $64 \times 64$ )	10.84
	Ours ( $256 \times 256$ )	14.87
	DDPM ( $256 \times 256$ ) [26]	7.89
	ProgressiveGAN ( $256 \times 256$ ) [31]	6.42

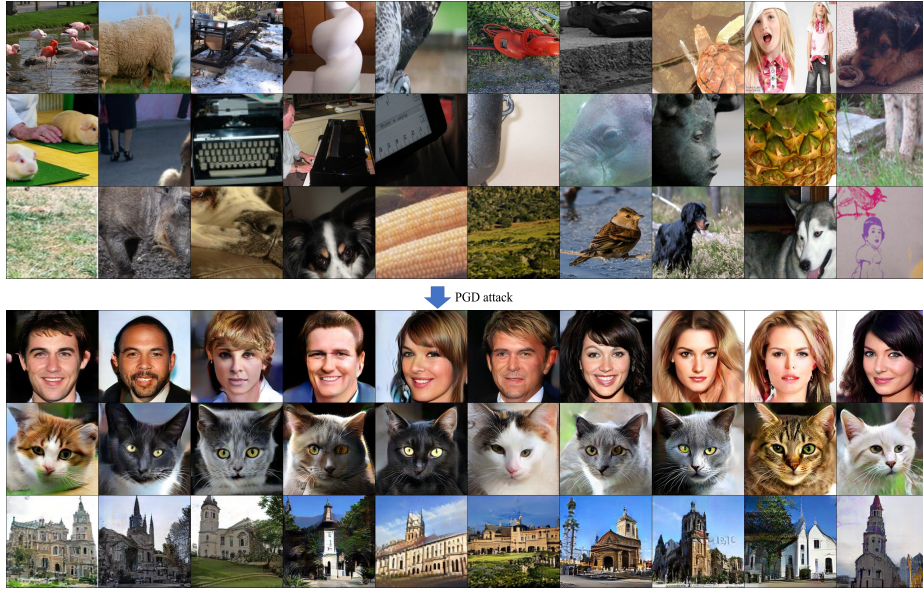


**Fig. 6.** Source images (top panel) and generated images (bottom panel,  $256 \times 256$  resolution) on CelebA-HQ, AFHQ-CAT, and LSUN Church.

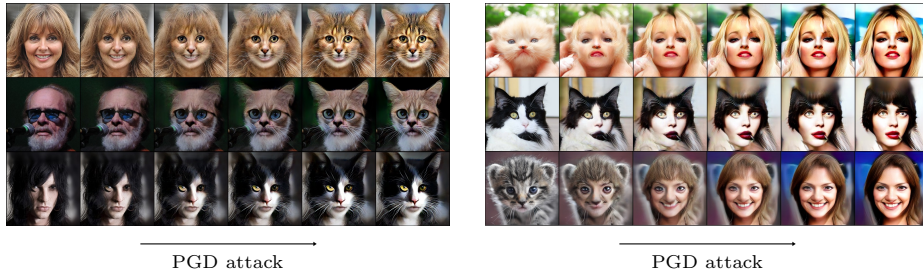


**Fig. 7.** Image-to-image translation demonstration

## 5.2 Applications

**Image-To-Image Translation.** Fig. 7 shows that the AFHQ-CAT model can be used to transform CelebA-HQ images into cat images, and vice-versa. Note that these two models are trained independently without knowledge of the source domain, indicating that our approach may generalize better to unseen data than approaches (e.g., pix2pix [29], CycleGAN [72], and StarGAN [6]) that explicitly use the source domain dataset to train the model. The translation results may be further improved by finetuning the trained model on the source domain dataset, or including the source domain data in the  $p_0$  dataset during training. The proposed approach is also more flexible than approaches that employs a fixed

generator, as it allows the user to choose how much transformation to apply, and/or create cinematic effect from intermediate transformation results.

**Worst-Case Out-Of-Distribution Detection.** Out-of-distribution (OOD) detection is a classic application of EBMs. Some recent works [52,39,3,2] find that EBMs and some other OOD detection approaches such as OE [24] are vulnerable to adversarial OOD inputs. Given the challenge of adversarial inputs, many authors attempt to address OOD detection in an adversarial setting (also known as worst-case, or adversarial OOD detection) [52,23,39,3,2]. Among these works, RATIO [2] is a state-of-the-art method that combines in- and out-distribution adversarial training to obtain a robust classifier that has uniform outputs in a neighborhood around OOD samples. Similar to OE, RATIO employs 80 million tiny images [56] as the out-distribution dataset to train the model.

Tab. 4 shows that our model achieves comparable OOD detection performance to the state-of-the-art method of RATIO [2]. OE, RATIO, and JEM all perform OOD detection by utilizing a classifier that has low confidence predictions on the out-distribution data (clean or worst-case). In RATIO, the worst-case out-distribution data is computed by performing the PGD attack on 80 million tiny images, whereas in JEM it is computed via Langevin dynamics initialized from uniform random noise. RATIO and our method’s strong out-distribution adversarial robustness demonstrates the benefit of using a real and diverse out-distribution dataset to train the model. Our method does not make use of class labels and therefore can be considered as a binary variant of RATIO. On CelebA-HQ 256, AFHQ-CAT, and LSUN-Church our model similarly achieves strong out-distribution adversarial robustness (supplementary materials). These results suggest that our generative model can be applied to detect both naturally occurring OOD data and adversarially created malicious content.

### 5.3 Training Stability Analysis

To gain some insight into the training stability of our approach we investigate whether the PGD attack can be used with the EBMs training objective Eq. (2). Specifically, in Algorithm 2, we perform step 5’s update on  $\theta$  using the gradient  $\nabla_{\theta}(\frac{1}{m} \sum_{i=1}^m f_{\theta}(x_i) - \frac{1}{m} \sum_{i=1}^m f_{\theta}(x_i^*))$ . We observe that even under a small learning rate of  $1e-6$ ,  $\frac{1}{m} \sum_{i=1}^m f_{\theta}(x_i) - \frac{1}{m} \sum_{i=1}^m f_{\theta}(x_i^*)$  quickly increases and eventually overflows. This suggests that the stability of the AT approach can be largely attributed to the log-likelihood objective Eq. (11). We argue that the stability is due to the gradient cancelling effect of this objective: when  $f_{\theta}$  has a large positive output on a sample  $x \sim p_{\text{data}}$ ,  $1 - \sigma(f_{\theta}(x))$  approaches 0 and therefore the corresponding scaled gradient in Eq. (14) vanishes, and similarly  $\sigma(f_{\theta}(x^*))\nabla_{\theta}f_{\theta}(x^*)$  vanishes when  $f_{\theta}$  has a large negative output on a sample  $x^* \sim p_T^*$ . In contrast, the EBMs objective Eq. (2) does not have constraints on  $f_{\theta}$ ’s outputs and is therefore prone to divergence.

**Table 4.** CIFAR-10 standard and worst-case OOD detection results (AUC scores). We use the same settings of AutoAttack [7], number of OOD samples, and perturbation limit as in [2] to compute adversarial OOD samples. Results of OE, JEM, and RATIO are from [2].

OOD dataset	Classifier-based approach			Ours
	OE [24]	JEM [16]	RATIO [2]	
Standard OOD detection				
SVHN	99.4	89.3	96.5	93.5
CIFAR-100	91.4	87.6	91.6	88.7
ImageNet	89.8	86.7	91.3	89.7
Uniform Noise	99.5	11.8	99.9	100
Worst-case OOD detection				
SVHN	0.6	7.3	81.3	83.0
CIFAR-100	2.7	19.2	73.0	70.6
ImageNet	1.5	21.2	73.5	72.5
Uniform Noise	43.1	2.5	99.8	100

## 6 Conclusion

We have studied an AT-based approach to learning EBMs. Our analysis shows that binary AT learns a special kind of energy function that models the support of the observed data, and the training procedure can be viewed as an approximate maximum likelihood learning algorithm. We proposed improved techniques for generative modeling with AT, and demonstrated that the proposed method provides competitive generation performance to explicit EBMs, has competitive sampling efficiency, is stable to train, and is well-suited for image translation tasks. The proposed approach’s strong out-distribution adversarial robustness suggests its potential application to detecting abnormal inputs and/or adversarially created fake content.

## References

1. Arbel, M., Zhou, L., Gretton, A.: Generalized energy based models. In: International Conference on Learning Representations (2021), <https://openreview.net/forum?id=OPtUPB9z6qK> 3
2. Augustin, M., Meinke, A., Hein, M.: Adversarial robustness on in-and out-distribution improves explainability. In: European Conference on Computer Vision. pp. 228–245. Springer (2020) 14, 15, 25, 26
3. Bitterwolf, J., Meinke, A., Hein, M.: Certifiably adversarially robust detection of out-of-distribution data. *Advances in Neural Information Processing Systems* **33** (2020) 14
4. Brock, A., Donahue, J., Simonyan, K.: Large scale GAN training for high fidelity natural image synthesis. In: International Conference on Learning Representations (2019), <https://openreview.net/forum?id=B1xsqj09Fm> 12, 27
5. Ceylan, C., Gutmann, M.U.: Conditional noise-contrastive estimation of unnormalised models. In: International Conference on Machine Learning. pp. 726–734. PMLR (2018) 4
6. Choi, Y., Uh, Y., Yoo, J., Ha, J.W.: Stargan v2: Diverse image synthesis for multiple domains. In: Proceedings of the IEEE/CVF Conference on Computer Vision and Pattern Recognition. pp. 8188–8197 (2020) 12, 13, 24, 25
7. Croce, F., Hein, M.: Reliable evaluation of adversarial robustness with an ensemble of diverse parameter-free attacks. In: ICML (2020) 15, 28
8. Cubuk, E.D., Zoph, B., Mane, D., Vasudevan, V., Le, Q.V.: Autoaugment: Learning augmentation strategies from data. In: Proceedings of the IEEE/CVF Conference on Computer Vision and Pattern Recognition. pp. 113–123 (2019) 25
9. Deng, J., Dong, W., Socher, R., Li, L.J., Li, K., Fei-Fei, L.: Imagenet: A large-scale hierarchical image database. In: 2009 IEEE conference on computer vision and pattern recognition. pp. 248–255. Ieee (2009) 26
10. Du, Y., Li, S., Mordatch, I.: Compositional visual generation with energy based models. *Advances in Neural Information Processing Systems* **33**, 6637–6647 (2020) 11, 28, 43
11. Du, Y., Li, S., Tenenbaum, J.B., Mordatch, I.: Improved contrastive divergence training of energy based models. In: ICML (2021) 1, 3, 12
12. Du, Y., Mordatch, I.: Implicit generation and modeling with energy based models. In: *Advances in Neural Information Processing Systems*. vol. 32 (2019), <https://proceedings.neurips.cc/paper/2019/file/378a063b8fdb1db941e34f4bde584c7d-Paper.pdf> 1, 3, 5, 12
13. Engstrom, L., Ilyas, A., Santurkar, S., Tsipras, D., Tran, B., Madry, A.: Adversarial robustness as a prior for learned representations. *arXiv preprint arXiv:1906.00945* (2019) 2
14. Gao, R., Song, Y., Poole, B., Wu, Y.N., Kingma, D.P.: Learning energy-based models by diffusion recovery likelihood. In: International Conference on Learning Representations (2021), [https://openreview.net/forum?id=v\\_1Soh8QUNc](https://openreview.net/forum?id=v_1Soh8QUNc) 12
15. Goodfellow, I., Pouget-Abadie, J., Mirza, M., Xu, B., Warde-Farley, D., Ozair, S., Courville, A., Bengio, Y.: Generative adversarial nets. In: *Advances in neural information processing systems*. pp. 2672–2680 (2014) 7, 22, 23
16. Grathwohl, W., Wang, K.C., Jacobsen, J.H., Duvenaud, D., Norouzi, M., Swersky, K.: Your classifier is secretly an energy based model and you should treat it like one. In: International Conference on Learning Representations (2020), <https://openreview.net/forum?id=HkzxxONtDB> 1, 3, 5, 12, 15, 26

17. Grathwohl, W.S., Kelly, J.J., Hashemi, M., Norouzi, M., Swersky, K., Duvenaud, D.: No mcmc for me: Amortized sampling for fast and stable training of energy-based models. In: International Conference on Learning Representations (2021), <https://openreview.net/forum?id=ixpSx09flk3> 1, 3, 12
18. Gulrajani, I., Ahmed, F., Arjovsky, M., Dumoulin, V., Courville, A.C.: Improved training of wasserstein gans. In: Advances in Neural Information Processing Systems. vol. 30 (2017), <https://proceedings.neurips.cc/paper/2017/file/892c3b1c6dccc52936e27cbd0ff683d6-Paper.pdf> 12
19. Gutmann, M., Hyvärinen, A.: Noise-contrastive estimation: A new estimation principle for unnormalized statistical models. In: Proceedings of the thirteenth international conference on artificial intelligence and statistics. pp. 297–304. JMLR Workshop and Conference Proceedings (2010) 3, 4
20. Han, T., Nijkamp, E., Fang, X., Hill, M., Zhu, S.C., Wu, Y.N.: Divergence triangle for joint training of generator model, energy-based model, and inferential model. In: Proceedings of the IEEE/CVF Conference on Computer Vision and Pattern Recognition. pp. 8670–8679 (2019) 3
21. Han, T., Nijkamp, E., Zhou, L., Pang, B., Zhu, S.C., Wu, Y.N.: Joint training of variational auto-encoder and latent energy-based model. In: Proceedings of the IEEE/CVF Conference on Computer Vision and Pattern Recognition. pp. 7978–7987 (2020) 3
22. He, K., Zhang, X., Ren, S., Sun, J.: Deep residual learning for image recognition. In: Proceedings of the IEEE conference on computer vision and pattern recognition. pp. 770–778 (2016) 24
23. Hein, M., Andriushchenko, M., Bitterwolf, J.: Why relu networks yield high-confidence predictions far away from the training data and how to mitigate the problem. In: Proceedings of the IEEE Conference on Computer Vision and Pattern Recognition. pp. 41–50 (2019) 14
24. Hendrycks, D., Mazeika, M., Dietterich, T.: Deep anomaly detection with outlier exposure. arXiv preprint arXiv:1812.04606 (2018) 14, 15, 26
25. Heusel, M., Ramsauer, H., Unterthiner, T., Nessler, B., Hochreiter, S.: Gans trained by a two time-scale update rule converge to a local nash equilibrium. In: Advances in neural information processing systems. pp. 6626–6637 (2017) 12, 25
26. Ho, J., Jain, A., Abbeel, P.: Denoising diffusion probabilistic models. In: Advances in Neural Information Processing Systems. vol. 33 (2020), <https://proceedings.neurips.cc/paper/2020/file/4c5bcfec8584af0d967f1ab10179ca4b-Paper.pdf> 3, 12
27. Hyvärinen, A., Dayan, P.: Estimation of non-normalized statistical models by score matching. *Journal of Machine Learning Research* **6**(4) (2005) 3
28. Ilyas, A., Santurkar, S., Tsipras, D., Engstrom, L., Tran, B., Madry, A.: Adversarial examples are not bugs, they are features. arXiv preprint arXiv:1905.02175 (2019) 2
29. Isola, P., Zhu, J.Y., Zhou, T., Efros, A.A.: Image-to-image translation with conditional adversarial networks. In: Proceedings of the IEEE conference on computer vision and pattern recognition. pp. 1125–1134 (2017) 13
30. Jiang, Z., Chen, T., Chen, T., Wang, Z.: Robust pre-training by adversarial contrastive learning. *Advances in Neural Information Processing Systems* **33**, 16199–16210 (2020) 4
31. Karras, T., Aila, T., Laine, S., Lehtinen, J.: Progressive growing of gans for improved quality, stability, and variation. arXiv preprint arXiv:1710.10196 (2017) 12, 25



32. Karras, T., Aittala, M., Hellsten, J., Laine, S., Lehtinen, J., Aila, T.: Training generative adversarial networks with limited data. In: Advances in Neural Information Processing Systems. vol. 33, pp. 12104–12114 (2020), <https://proceedings.neurips.cc/paper/2020/file/8d30aa96e72440759f74bd2306c1fa3d-Paper.pdf> 12, 25
33. Kingma, D.P., Dhariwal, P.: Glow: Generative flow with invertible 1x1 convolutions. In: Advances in neural information processing systems. pp. 10215–10224 (2018) 12
34. Krizhevsky, A., Hinton, G., et al.: Learning multiple layers of features from tiny images (2009) 12, 25
35. Kumar, R., Ozair, S., Goyal, A., Courville, A., Bengio, Y.: Maximum entropy generators for energy-based models. arXiv preprint arXiv:1901.08508 (2019) 3
36. Kurakin, A., Goodfellow, I., Bengio, S.: Adversarial machine learning at scale. arXiv preprint arXiv:1611.01236 (2016) 5
37. LeCun, Y., Chopra, S., Hadsell, R., Ranzato, M., Huang, F.: A tutorial on energy-based learning. Predicting structured data 1(0) (2006) 1, 4
38. Madry, A., Makelov, A., Schmidt, L., Tsipras, D., Vladu, A.: Towards deep learning models resistant to adversarial attacks. arXiv preprint arXiv:1706.06083 (2017) 5, 10
39. Meinke, A., Hein, M.: Towards neural networks that provably know when they don’t know. arXiv preprint arXiv:1909.12180 (2019) 14
40. Mescheder, L., Geiger, A., Nowozin, S.: Which training methods for gans do actually converge? In: International conference on machine learning. pp. 3481–3490. PMLR (2018) 11
41. Miyato, T., Kataoka, T., Koyama, M., Yoshida, Y.: Spectral normalization for generative adversarial networks. In: International Conference on Learning Representations (2018), <https://openreview.net/forum?id=B1QRgziT-> 12
42. Nijkamp, E., Gao, R., Sountsov, P., Vasudevan, S., Pang, B., Zhu, S.C., Wu, Y.N.: MCMC should mix: Learning energy-based model with flow-based backbone. In: International Conference on Learning Representations (2022), <https://openreview.net/forum?id=4C93Qvn-tz> 3
43. Nijkamp, E., Hill, M., Han, T., Zhu, S.C., Wu, Y.N.: On the anatomy of mcmc-based maximum likelihood learning of energy-based models. In: Proceedings of the AAAI Conference on Artificial Intelligence. vol. 34, pp. 5272–5280 (2020) 1, 2, 3, 5, 9
44. Nijkamp, E., Hill, M., Zhu, S.C., Wu, Y.N.: Learning non-convergent non-persistent short-run mcmc toward energy-based model. In: NeurIPS (2019) 1, 2, 3, 5, 12
45. Pang, B., Han, T., Nijkamp, E., Zhu, S.C., Wu, Y.N.: Learning latent space energy-based prior model. In: Advances in Neural Information Processing Systems. vol. 33 (2020), <https://proceedings.neurips.cc/paper/2020/file/fa3060edb66e6ff4507886f9912e1ab9-Paper.pdf> 3
46. Pidhorskyi, S., Adjeroh, D.A., Doretto, G.: Adversarial latent autoencoders. In: Proceedings of the IEEE/CVF Conference on Computer Vision and Pattern Recognition. pp. 14104–14113 (2020) 12
47. Ramachandran, P., Zoph, B., Le, Q.V.: Swish: a self-gated activation function. arXiv preprint arXiv:1710.05941 7, 1 (2017) 3
48. Rhodes, B., Xu, K., Gutmann, M.U.: Telescoping density-ratio estimation. arXiv preprint arXiv:2006.12204 (2020) 4
49. Salimans, T., Goodfellow, I., Zaremba, W., Cheung, V., Radford, A., Chen, X.: Improved techniques for training gans. Advances in neural information processing systems 29, 2234–2242 (2016) 12, 25



50. Salimans, T., Kingma, D.P.: Weight normalization: A simple reparameterization to accelerate training of deep neural networks. *Advances in neural information processing systems* **29**, 901–909 (2016) [3](#)
51. Santurkar, S., Ilyas, A., Tsipras, D., Engstrom, L., Tran, B., Madry, A.: Image synthesis with a single (robust) classifier. In: *Advances in Neural Information Processing Systems*. pp. 1260–1271 (2019) [2](#), [12](#)
52. Sehwag, V., Bhagoji, A.N., Song, L., Sitawarin, C., Cullina, D., Chiang, M., Mittal, P.: Better the devil you know: An analysis of evasion attacks using out-of-distribution adversarial examples. *arXiv preprint arXiv:1905.01726* (2019) [14](#)
53. Song, Y., Ermon, S.: Generative modeling by estimating gradients of the data distribution. In: *Advances in Neural Information Processing Systems*. vol. 32 (2019), <https://proceedings.neurips.cc/paper/2019/file/3001ef257407d5a371a96dcd947c7d93-Paper.pdf> [3](#), [12](#), [27](#)
54. Song, Y., Ermon, S.: Improved techniques for training score-based generative models. *arXiv preprint arXiv:2006.09011* (2020) [3](#), [12](#)
55. Song, Y., Sohl-Dickstein, J., Kingma, D.P., Kumar, A., Ermon, S., Poole, B.: Score-based generative modeling through stochastic differential equations. In: *International Conference on Learning Representations* (2021), <https://openreview.net/forum?id=PXTIG12RRHS> [3](#), [12](#)
56. Torralba, A., Fergus, R., Freeman, W.T.: 80 million tiny images: A large data set for nonparametric object and scene recognition. *IEEE transactions on pattern analysis and machine intelligence* **30**(11), 1958–1970 (2008) [14](#), [26](#)
57. Tsipras, D., Santurkar, S., Engstrom, L., Turner, A., Madry, A.: Robustness may be at odds with accuracy. *arXiv preprint arXiv:1805.12152* (2018) [2](#)
58. Vahdat, A., Kautz, J.: Nvae: A deep hierarchical variational autoencoder. In: *Advances in Neural Information Processing Systems*. vol. 33 (2020), <https://proceedings.neurips.cc/paper/2020/file/e3b21256183cf7c2c7a66be163579d37-Paper.pdf> [12](#), [27](#)
59. Wang, Y., Wang, Y., Yang, J., Lin, Z.: A unified contrastive energy-based model for understanding the generative ability of adversarial training. In: *International Conference on Learning Representations* (2022), <https://openreview.net/forum?id=XhF2VOMRHS> [4](#), [12](#)
60. Welling, M., Teh, Y.W.: Bayesian learning via stochastic gradient langevin dynamics. In: *Proceedings of the 28th international conference on machine learning (ICML-11)*. pp. 681–688. Citeseer (2011) [3](#), [5](#)
61. Xiao, Z., Kreis, K., Kautz, J., Vahdat, A.: Vaebm: A symbiosis between variational autoencoders and energy-based models. In: *International Conference on Learning Representations* (2021), <https://openreview.net/forum?id=5m3SEcz0V8L> [1](#), [3](#), [12](#), [26](#), [27](#)
62. Xie, J., Lu, Y., Gao, R., Zhu, S.C., Wu, Y.N.: Cooperative training of descriptor and generator networks. *IEEE transactions on pattern analysis and machine intelligence* **42**(1), 27–45 (2018) [3](#)
63. Xie, J., Lu, Y., Zhu, S.C., Wu, Y.: A theory of generative convnet. In: *International Conference on Machine Learning*. pp. 2635–2644. PMLR (2016) [3](#), [5](#)
64. Xie, J., Zheng, Z., Fang, X., Zhu, S.C., Wu, Y.N.: Cooperative training of fast thinking initializer and slow thinking solver for conditional learning. *IEEE Transactions on Pattern Analysis and Machine Intelligence* (2021) [4](#)
65. Xie, J., Zheng, Z., Gao, R., Wang, W., Zhu, S.C., Wu, Y.N.: Learning descriptor networks for 3d shape synthesis and analysis. In: *Proceedings of the IEEE conference on computer vision and pattern recognition*. pp. 8629–8638 (2018) [4](#)

66. Xie, J., Zheng, Z., Gao, R., Wang, W., Zhu, S.C., Wu, Y.N.: Generative voxelnet: learning energy-based models for 3d shape synthesis and analysis. *IEEE Transactions on Pattern Analysis and Machine Intelligence* (2020) [4](#)
67. Xie, J., Zheng, Z., Li, P.: Learning energybased model with variational auto-encoder as amortized sampler. In: *The Thirty-Fifth AAAI Conference on Artificial Intelligence (AAAI)*. vol. 2 (2021) [3](#), [12](#)
68. Xie, J., Zhu, Y., Li, J., Li, P.: A tale of two flows: Cooperative learning of langevin flow and normalizing flow toward energy-based model. In: *International Conference on Learning Representations* (2022), <https://openreview.net/forum?id=31d5RLCUuXC> [3](#), [12](#)
69. Yin, X., Kolouri, S., Rohde, G.K.: Gat: Generative adversarial training for adversarial example detection and robust classification. In: *International Conference on Learning Representations* (2020), <https://openreview.net/forum?id=SJeQE4YDH> [2](#), [5](#)
70. Yu, F., Seff, A., Zhang, Y., Song, S., Funkhouser, T., Xiao, J.: Lsun: Construction of a large-scale image dataset using deep learning with humans in the loop. *arXiv preprint arXiv:1506.03365* (2015) [12](#), [25](#)
71. Zhao, Y., Xie, J., Li, P.: Learning energy-based generative models via coarse-to-fine expanding and sampling. In: *International Conference on Learning Representations* (2021), [https://openreview.net/forum?id=aD1\\_5zowqV](https://openreview.net/forum?id=aD1_5zowqV) [1](#), [3](#), [12](#), [26](#)
72. Zhu, J.Y., Park, T., Isola, P., Efros, A.A.: Unpaired image-to-image translation using cycle-consistent adversarial networks. In: *Proceedings of the IEEE international conference on computer vision*. pp. 2223–2232 (2017) [13](#)
73. Zhu, Y., Ma, J., Sun, J., Chen, Z., Jiang, R., Chen, Y., Li, Z.: Towards understanding the generative capability of adversarially robust classifiers. In: *Proceedings of the IEEE/CVF International Conference on Computer Vision*. pp. 7728–7737 (2021) [4](#), [12](#)

# Supplementary Materials

## 1 Proof of Proposition (1)

**Proposition 1.** *The optimal solution of  $\max_D \min_{p_T} U(D, p_T)$  is  $U(D^*, p_T^*) = -\log(4)$ , where  $D^*$  outputs  $\frac{1}{2}$  on  $\text{Supp}(p_{\text{data}})$  and  $\leq \frac{1}{2}$  outside  $\text{Supp}(p_{\text{data}})$ , and  $p_T^*$  is supported in the contour set  $\{D = \frac{1}{2}\}$ .*

*Proof.* Let

$$p_T^* = \arg \min_{p_T} \mathbb{E}_{x \sim p_T} [\log(1 - D(x))], \quad (1)$$

then

$$\max_D \min_{p_T} U(D, p_T) = \max_D U(D, p_T^*). \quad (2)$$

We solve  $\max_D U(D, p_T^*)$  by first deriving its upper bound. Let  $\alpha = \max_{\mathcal{X}} D$ , then  $\mathbb{E}_{x \sim p_T^*} [\log(1 - D(x))]$  is minimized when  $p_T^*$  is supported in  $\{x : D(x) = \alpha\}$ . With this result, we can derive an upper bound of  $U(D, p_T^*)$ :

$$\begin{aligned} U(D, p_T^*) &= \int_{\mathcal{X}} p_{\text{data}}(x) \log D(x) dx + \int_{\mathcal{X}} p_T^*(x) \log(1 - D(x)) dx \\ &= \int_{\mathcal{X}} p_{\text{data}}(x) \log D(x) dx + \int_{\mathcal{X}} p_T^*(x) \log(1 - \alpha) dx \\ &\leq \int_{\mathcal{X}} p_{\text{data}}(x) \log(\alpha) dx + \int_{\mathcal{X}} p_T^*(x) \log(1 - \alpha) dx \\ &= \log(\alpha) + \log(1 - \alpha) \\ &\leq -\log(4), \end{aligned} \quad (3)$$

where the last inequality follows from the fact that the function  $f(\alpha) = \log(\alpha) + \log(1 - \alpha)$  achieves its maximum value of  $-\log(4)$  at  $\alpha = \frac{1}{2}$ . It is not hard to see that equality holds if and only if i)  $\max_{\mathcal{X}} D = \frac{1}{2}$ , ii)  $D = \frac{1}{2}$  on  $\text{Supp}(p_{\text{data}})$ , and iii)  $\text{Supp}(p_T^*) \subseteq \{x : D(x) = \frac{1}{2}\}$ . In summary,  $\max_D \min_{p_T} U(D, p_T)$  achieves its optimal value of  $-\log(4)$  at  $(D^*, p_T^*)$  where

$$D^*(x) = \begin{cases} \frac{1}{2} & x \in \text{Supp}(p_{\text{data}}) \\ \leq \frac{1}{2} & x \in \mathcal{X} \setminus \text{Supp}(p_{\text{data}}) \end{cases}, \quad (4)$$

and  $p_T^*$  is supported in the contour set  $\{D = \frac{1}{2}\}$ .

## 2 Connection to GANs

In this section we provide a comparative analysis of the proposed AT generative model and GANs [15]. The proposed approach learns data distribution by solving the maximin problem

$$\max_D \min_{p_T} U(D, p_T) = \mathbb{E}_{x \sim p_{\text{data}}} [\log D(x)] + \mathbb{E}_{x \sim p_T} [\log(1 - D(x))], \quad (5)$$

while GANs learn a generator function  $G$  by solving the minimax problem

$$\min_G \max_D V(D, G) = \mathbb{E}_{x \sim p_{\text{data}}} [\log D(x)] + \mathbb{E}_{z \sim p_z} [\log(1 - D(G(z)))]. \quad (6)$$

The generator  $G$  implicitly defines a distribution  $p_g$  by mapping a prior distribution  $p_z$  from a low-dimensional latent space  $\mathcal{Z} \subseteq \mathbb{R}^z$  to the high-dimensional data space  $\mathcal{X} \subseteq \mathbb{R}^d$ . Plugging  $p_g$  into Eq. (6), we get:

$$\min_{p_g} \max_D U(D, p_g) = \mathbb{E}_{x \sim p_{\text{data}}} [\log D(x)] + \mathbb{E}_{x \sim p_g} [\log(1 - D(x))] \quad (7)$$

Comparing Eq. (5) with Eq. (7) we find both problems making use of the standard log-likelihood objective for binary classification, but have a reversed order of minimization and maximization. In fact, both formulations solve a two-player zero-sum game, a mathematical representation of a situation in which one player's gain is balanced by another player's loss. This game can be described by the *payoff function*  $f : \mathbb{R}^{p+q} \rightarrow \mathbb{R}$ , which represents the amount of payment that one player (player 1) makes to the other player (player 2). The goal of player 1 is to choose a strategy  $u \in \mathbb{R}^p$  such that the payoff is minimized, while the goal of player 2 is to choose a strategy  $v \in \mathbb{R}^q$  such that the payoff is maximized. Depending on the order of maximization and minimization, the best strategies for both players, and the optimal payoff, can be solved via  $\min_u \max_v f(u, v)$  or  $\max_v \min_u f(u, v)$ .

In Eq. (5),  $U(D, p_T)$  is the payoff function, and the goal of player  $p_T$  is to choose a strategy  $p_T^*$  such that the payoff is minimized, whereas the goal of player  $D$  is to choose a strategy  $D^*$  such that the payoff is maximized. This *maximin* game is played by following such a rule: player  $D$  makes the first move by choosing a  $D$ ; player  $p_T$ , after learning that player  $D$  has made the move, will choose a  $p_T$  to minimize its payment, which results in a payoff of  $\min_{p_T} U(D, p_T)$ ; player  $D$ , who is informed of player  $p_T$ 's strategy, will choose a  $D$  such that the worst case payoff  $\min_{p_T} U(D, p_T)$  is maximized, which results in an overall payoff of  $\max_D \min_{p_T} U(D, p_T)$ . The best strategies of both players and the maximum payoff can be derived from Proposition 1: In the maximin game  $\max_D \min_{p_T} U(D, p_T)$ , the best strategy for player  $D$  is to choose a  $D^*$  that outputs  $\frac{1}{2}$  on  $\text{Supp}(p_{\text{data}})$  and  $\leq \frac{1}{2}$  outside  $\text{Supp}(p_{\text{data}})$ , the best strategy for player  $p_T$  is to choose a  $p_T^*$  which is supported in  $\{x : D(x) = \frac{1}{2}\}$ , and the maximum payoff is  $-\log(4)$ .

In Eq. (7),  $U(D, p_g)$  is the payoff function. Similar to Eq. (5), the goal of player  $p_g$  is to minimize the payoff, and the goal of player  $D$  is to maximize

the payoff. In contrast to Eq. (5), player  $p_g$  makes the first move. The solution to this minimax game is analyzed in [15]: the best strategy of player  $p_g$  is to choose a  $p_g^*$  which minimizes the Jensen-Shannon divergence (JSD) between  $p_g$  and  $p_{\text{data}}$ :  $p_g^* = \arg \min_{p_g} \text{JSD}(p_g \parallel p_{\text{data}}) = p_{\text{data}}$ , and the best strategy of player  $D$  is to choose  $D^*(x) = \frac{p_{\text{data}}(x)}{p_{\text{data}}(x) + p_g^*(x)} = \frac{1}{2}$ . Under these strategies, the payoff function  $U$  measures the JSD between  $p_g$  and  $p_{\text{data}}$ :  $U(D^*, p_g^*) = -\log(4) + 2 \cdot \text{JSD}(p_g^* \parallel p_{\text{data}}) = -\log(4)$ , which coincides with the  $U$  solution in the maximin game. Note that in the minimax game,  $D^*$  does not need to be defined outside  $\text{Supp}(p_g) \cup \text{Supp}(p_{\text{data}})$  [15].

The optimal solutions to these two formulations are summarized in Tab. 1.

The pseudo code for solving the minimax problem is outlined in Algorithm 3. Fig. 1 shows the simulation results in two settings where  $p_0$  data is respectively uniformly distributed (left panel) and concentrated in the lower left corner (right panel). It can be seen that in both cases  $p_T^*$  matches  $p_{\text{data}}$  when the algorithm converges. The right panel shows that when  $p_0$  data is concentrated in the lower left corner, the  $D$  solution has undefined outputs outside  $\text{Supp}(p_{\text{data}})$ .

We find these two formulations giving rise to different applications. The minimax formulation is ideal for learning a generator model that can produce a distribution that matches  $p_{\text{data}}$ . The discriminator, because of its undefined behavior outside  $\text{Supp}(p_{\text{data}})$ , may not be very useful for some downstream tasks such as out-of-distribution detection. In the maximin formulation, as we have discussed in the main text, can be used for sample generation, image-to-image translation, image restoration such as denoising and inpainting, and (worst-case) out-of-distribution detection.

**Table 1.** Optimal solutions to the minimax problem and maximin problem

	Minimax (GANs) Eq. (7)	Maximin (ours) Eq. (5)
$p_T^*/p_g^*$	$p_g^* = p_{\text{data}}$	$p_T^*$ is supported in $\{x : D(x) = \frac{1}{2}\}$
$D^*$	$D^*(x) = \frac{1}{2}$ on $\text{Supp}(p_{\text{data}})$ , undefined outside $\text{Supp}(p_{\text{data}})$	$D^*(x) = \frac{1}{2}$ on $\text{Supp}(p_{\text{data}})$ , $D^*(x) \leq \frac{1}{2}$ outside $\text{Supp}(p_{\text{data}})$
$U(D^*, p_g^*)/U(D^*, p_T^*)$	$-\log(4)$	$-\log(4)$

**Algorithm 3** Solving the minimax problem

- 
- 1: Draw samples  $\{x_i\}_{i=1}^m$  from  $p_{\text{data}}$ , and samples  $\{x_i^*\}_{i=1}^m$  from  $p_0$ .
  - 2: **repeat**
  - 3:   Update  $D$  by maximizing  $\frac{1}{m} \sum_{i=1}^m \log D(x_i) + \frac{1}{m} \sum_{i=1}^m \log(1 - D(x_i^*))$  (until converge).
  - 4:   For each  $x \in \{x_i^*\}_{i=1}^m$ , update its value by  

$$x \leftarrow x + \lambda \frac{\nabla D(x)}{\|\nabla D(x)\|_2} \quad (\text{single step}).$$
  - 5: **until**  $\{x_i^*\}_{i=1}^m = \{x_i\}_{i=1}^m$
- 

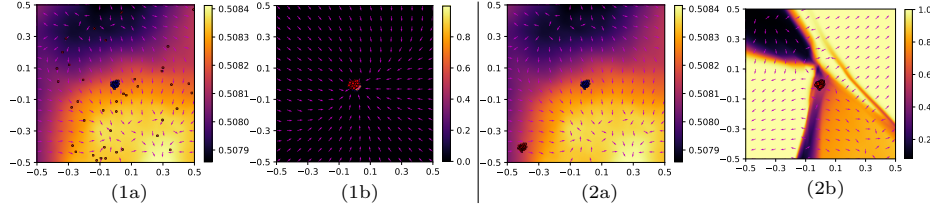


**Fig. 1.** Plots of contours and (normalized) gradient vector fields of the  $D$  functions learned with different  $p_0$  data. Left and right panel respectively show the initial state (1a and 2a) and final state (1b and 2b) of  $D$  when  $p_0$  data is respectively uniformly distributed (red points in 1a) and concentrated in the lower left corner (red points in 2a).  $p_{\text{data}}$  is a Gaussian distribution centered at  $(0, 0)$  (blue points).

### 3 Experimental Setups

**Model Architecture.** On CIFAR-10 we use the standard ResNet50 [22] architecture with ReLU activation for the  $D$  model. On CelebA-HQ 256, AFHQ-CAT 256, and LSUN-Church 256 we use a customized architecture (Tab. 2) adapted from [6].

**Table 2.** Network architecture for the  $D$  model used in CelebA-HQ 256, AFHQ-CAT 256, and LSUN-Church 256.

Layer	Resample	Output shape
Conv1 × 1	-	256 × 256 × 64
ResBlock	AvgPool	128 × 128 × 128
ResBlock	AvgPool	64 × 64 × 256
ResBlock	AvgPool	32 × 32 × 512
ResBlock	AvgPool	16 × 16 × 512
ResBlock	AvgPool	8 × 8 × 512
ResBlock	AvgPool	4 × 4 × 512
LeakyReLU	-	4 × 4 × 512
Conv4 × 4	-	1 × 1 × 512
LeakyReLU	-	1 × 1 × 512
Reshape	-	512
Linear	-	1

**Datasets.** We evaluate our method on CIFAR-10 [34] (50K training samples), CelebA-HQ 256 [31] (30K training samples), AFHQ-CAT [6] dataset (5153 training samples), and LSUN-Church [70] (126227 training samples). AFHQ [6] is a recently introduced benchmark dataset for image-to-image translation.

**Evaluation Metrics.** We use Inception Score (IS) [49] and FID score [25] to evaluate the quality of generated samples. We follow [32] and compute the FID score between 50k generated samples and all training samples (IS is also calculated on the generated 50K samples). We use the original code from [49] and [25] to calculate the scores. For OOD detection, we use area under the ROC curve (AUROC) as the evaluation metric.

**Training.** We use Algorithm 2 to train the models. The training hyperparameters for each task can be found in Tab. 3. For the  $256 \times 256$  tasks, we pretrain the  $D$  model on the ImageNet classification task. To mitigate overfitting, we perform random resized cropping, random horizontal flipping on  $p_{\text{data}}$  samples. The performance (FID score) of the model is monitored during training and the best-performing model is used to report the final FID score.

The CIFAR-10 worst-case OOD detection model is trained using in- and out-distribution adversarial training [2], where in-distribution AT uses a  $l^2$ -ball of radius 0.25 and PGD attacks of steps 10 and step-size 0.1, and out-distribution AT uses a  $l^2$ -ball of radius 0.5 and PGD attacks of steps 10 and step-size 0.1. Following [2], we use a batch size of 128 and use the recommended AutoAugment policy from [8]. The model is trained for 400 epochs using a SGD optimizer with a fixed learning rate of 0.1.

**Table 3.** Training hyperparameters. We use  $\beta_1 = 0.0, \beta_2 = 0.99$  for the Adam optimizer.

	CIFAR-10	CelebA-HQ 256	AFHQ-CAT 256	LSUN-Church 256
Batch size	32	40	40	32
Training iterations	172K	218K	225K	215K
Optimizer	Adam	Adam	Adam	Adam
Learning rate	5e-4	5e-5	5e-5	5e-5
$K$	0,...,25	0,...,40	0,...,25	0,...,35
Epochs per $K$	5	5	50	1
PGD attack step-size	0.1	2.0	2.0	2.0
$R_1$ regularization	0.01	30	100	100

**Sample Generation.** The generated samples for FID and IS evaluation are produced by performing PGD attacks on 50K samples randomly drawn from



the  $p_0$  dataset. The settings for the  $p_0$  dataset and the PGD attack can be found in Table 4.

**Table 4.** Sample generation setting

Task	$p_0$ dataset	PGD step size	PGD steps
CIFAR-10	80 million tiny images [56]	0.2	32
CelebA-HQ 256	ImageNet [9]	8.0	20
AFHQ-CAT 256	ImageNet [9]	8.0	14
LSUN-Church 256	ImageNet [9]	8.0	17

## 4 Extended Experiment Results

### 4.1 Training and Test Time Sampling Efficiency

Tab. 5 shows that our method has competitive training and test time sampling efficiency to state-of-the-art EBMs. Although VAEBM typically requires much fewer update steps than our method, its per-step efficiency is much worse (Tab. 6), suggesting that its VAE component has considerable computational complexity. We also observe that the quality of our generated samples is not sensitive to the number of sampling steps as long as the overall perturbation ( $\#step \times step\text{-size}$ ) remains the same (Tab. 7). This allows us to use a much larger step size than the one used during training to speedup test time sampling in real applications.

**Table 5.** The number of update steps in the PGD attack (our method) and Langevin dynamics (other methods). “PCD” refers to using a persistent sampling chain.

	Ours	VAEBM [61]	CF-EBM [71]	JEM [16]
CIFAR-10 (train)	25	6 (PCD)	50	20 (PCD)
CIFAR-10 (test)	32	16	50	100
CelebA-HQ 256 (train)	40	6 (PCD)	90	N/A
CelebA-HQ 256 (test)	20	24	90	N/A

### 4.2 Extend Results on Worst-Case Out-Of-Distribution Detection

Tab. 8 shows that under a PGD adversary with  $l^2$  radius 7.0 our model exhibits strong out-distribution robustness. (Note that according to [2], a perturbation of 7.0 is already large enough to make undefended models (e.g., OE [24]) fail completely at the OOD detection task).

**Table 6.** Number of steps and wall-clock time to generate 50 CIFAR-10 samples. Data of NCSN and VAEBM are from [61].

Model	Steps	Wall-clock time	GPU device
NCSN [53]	1000	107.9 seconds	RTX Titan
VAEBM [61]	16	8.79 seconds	RTX Titan
Ours	32	2.34 seconds	RTX 2080 Ti

**Table 7.** FID scores of samples generated using different combinations of number of steps and step-size.

	Number of steps $\times$ step-size	FID
CIFAR-10	$64 \times 0.1$	13.07
	$32 \times 0.2$	13.21
	$16 \times 0.4$	13.49
CelebA-HQ 256	$40 \times 4.0$	19.19
	$20 \times 8.0$	18.97
	$10 \times 16.0$	19.19

### 4.3 Extended Results on Generation

Additional results are summarized below:

- **Uncurated generation samples.** Fig. 2, Fig. 4, Fig. 6, and Fig. 7 show the uncurated generated samples on CIFAR-10, CelebA-HQ 256, AFHQ-CAT 256, and LSUN-Church 256. Note that we have used the same seed images (Fig. 21) to generated these results. We find that some generated images contain artifacts. By first applying Gaussian smoothing ( $\sigma = 10$ ) to the source images ( $p_0$  data), we are able to obtain more visually pleasing results (Fig. 5). The generated samples contain less artifacts, but have a slightly worse FID. The smoothing filters out high frequency components, and seems to be playing a similar role as reduced-temperature sampling [58,61] and the “truncation trick” [4], where better-looking results (typically with reduced diversity) can be generated from latent noise sampled from the high density area of the latent space.
- **Nearest Neighbor Analysis.** Fig. 3, Fig. 8, Fig. 9, and Fig. 10 show the pixel space and inception feature space nearest neighbors of the generated samples on CIFAR-10, CelebA-HQ 256, AFHQ-CAT 256, and LSUN-Church 256. Note that none of the nearest neighbors resemble the generated samples, suggesting that the models have not memorized the training data.
- **Interpolation.** Fig. 11, Fig. 12, and Fig. 13 show the interpolation results on CelebA-HQ 256, AFHQ-CAT 256, and LSUN-Church 256. The interpolation works reasonable well even on AFHQ-CAT where only about 5000 training images are available.

**Table 8.** OOD detection results on  $256 \times 256$  datasets. Each entry shows the AUC score on clean OOD samples (left value) and AUC score on adversarial OOD samples (right value). Adversarial OOD samples are computed by maximizing the model output in a  $l^2$ -ball of radius 7.0 around OOD samples via Auto-PGD [7] with 100 steps and 5 random restarts. Results are computed using 1024 in-distribution samples and 1024 out-distribution samples.

OOD dataset	In-distribution dataset		
	CelebA-HQ 256	AFHQ-CAT 256	LSUN-Church 256
Standard OOD detection			
Uniform noise	1.0	1.0	0.9476
SVHN	0.9967	0.9944	0.9668
CIFAR-10	0.9978	0.9930	0.9081
ImageNet validation set	0.9986	0.9971	0.9409
AFHQ-CAT 256	0.9984	N/A	0.9691
CelebA-HQ 256	N/A	0.9900	0.9794
LSUN-Church 256	0.9999	0.9997	N/A
Worst-case OOD detection			
Uniform noise	1.0	1.0	0.9330
SVHN	0.9928	0.9880	0.9566
CIFAR-10	0.9952	0.9859	0.8857
ImageNet validation set	0.9973	0.9937	0.9270
AFHQ-CAT 256	0.9958	N/A	0.9587
CelebA-HQ 256	N/A	0.9773	0.9714
LSUN-Church 256	0.9998	0.9991	N/A

- **Intermediate Generation Results.** Fig. 14, Fig. 15, and Fig. 16 show the intermediate generation results. It can be seen that the model is capable of transforming natural images into valid images of the target data distribution. In addition, when the number of PGD attack steps is too large, the generated samples become saturated, which suggests that the model, like many EBMs trained with short-run MCMC, do not have a valid steady-state that reflects the distribution of target data.
- **Compositional Visual Generation.** Fig. 17 shows that our model can be composed like regular EBMs [10].
- **Denosing and Inpainting.** Fig. 18 and Fig. 19 show uncured denoising and inpainting results on CelebA-HQ 256 and AFHQ-CAT 256.
- **Image Translation.** Fig. 20 shows uncured image translation results on CelebA-HQ 256 and AFHQ-CAT 256.

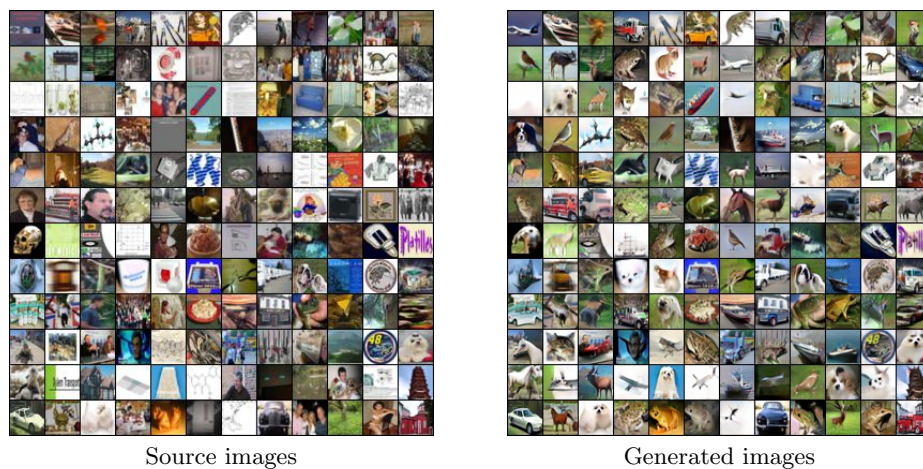


**Fig. 2.** Uncurated CIFAR-10 generated samples.

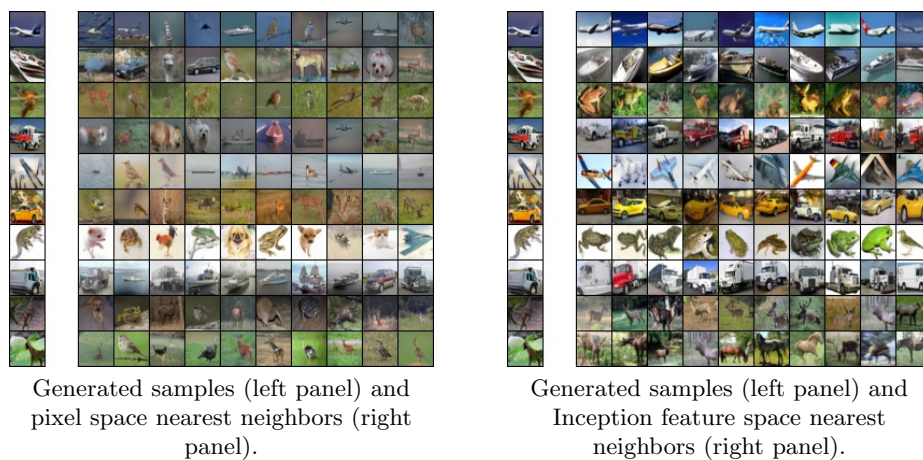


**Fig. 3.** Nearest neighbors of generated samples on CIFAR-10.





**Fig. 4.** Uncurated generated samples on CelebAHQ-256. Source images are in Fig. 21.



**Fig. 5.** Uncurated generated samples on CelebAHQ-256. The source images used to generate these samples are obtained by applying Gaussian blur ( $\sigma = 10$ ) to the images in Fig. 21.





**Fig. 6.** Uncurated generated samples on AFHQ-CAT 256. Source images are in Fig. 21.





**Fig. 7.** Uncurated generated samples on LSUN-Church 256. Source images are in Fig. 21.

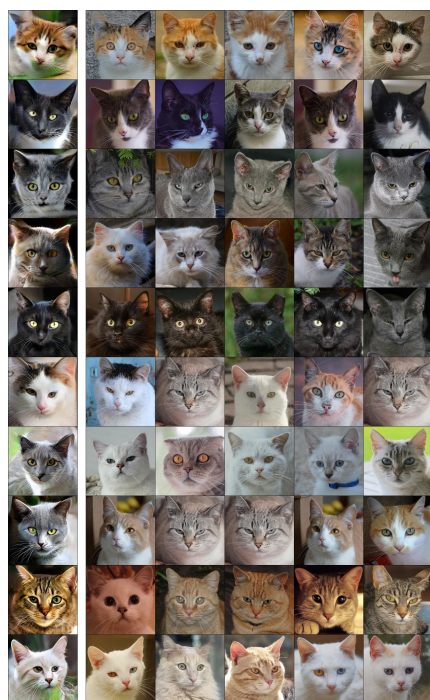


Generated samples (left panel) and  
pixel space nearest neighbors (right  
panel)

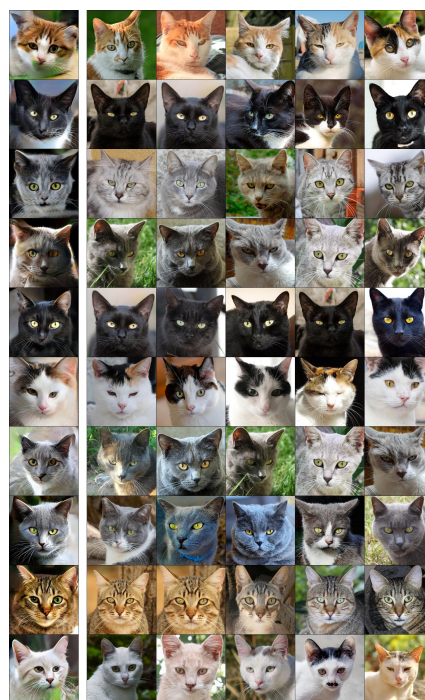


Generated samples (left panel) and  
Inception feature space nearest  
neighbors (right panel).

**Fig. 8.** Nearest neighbors of generated samples on CelebA-HQ 256.



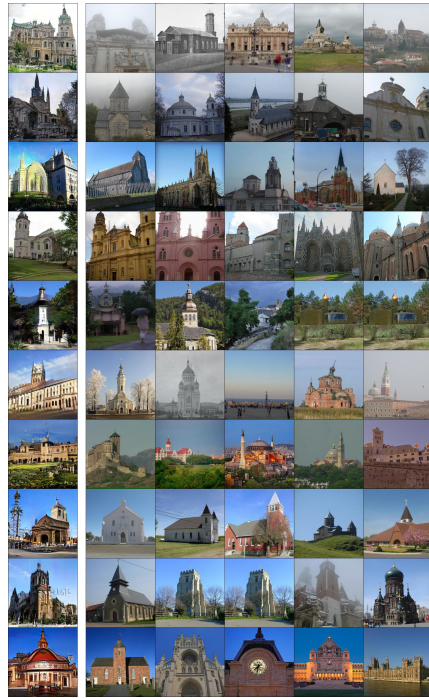
Generated samples (left panel) and pixel space nearest neighbors (right panel)



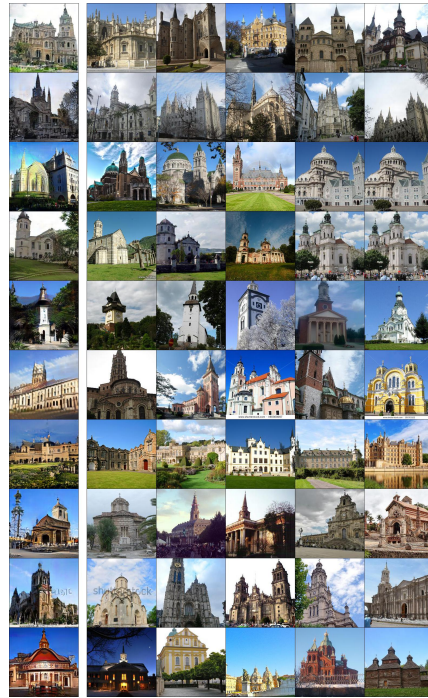
Generated samples (left panel) and Inception feature space nearest neighbors (right panel).

**Fig. 9.** Nearest neighbors of generated samples on AFHQ-CAT 256.





Generated samples (left panel) and  
pixel space nearest neighbors (right  
panel)



Generated samples (left panel) and  
Inception feature space nearest  
neighbors (right panel).

**Fig. 10.** Nearest neighbors of generated samples on LSUN-Church 256.



**Fig. 11.** Interpolation results on CelebA-HQ 256. Intermediate images are generated by performing PGD attacks on linear interpolations between the source images used to generate the leftmost and rightmost samples.





**Fig. 12.** Interpolation results on AFHQ-CAT 256. Intermediate images are generated by performing PGD attacks on linear interpolations between the source images used to generate the leftmost and rightmost samples.



**Fig. 13.** Interpolation results on LSUN-Church 256. Intermediate images are generated by performing PGD attacks on linear interpolations between the source images used to generate the leftmost and rightmost samples.



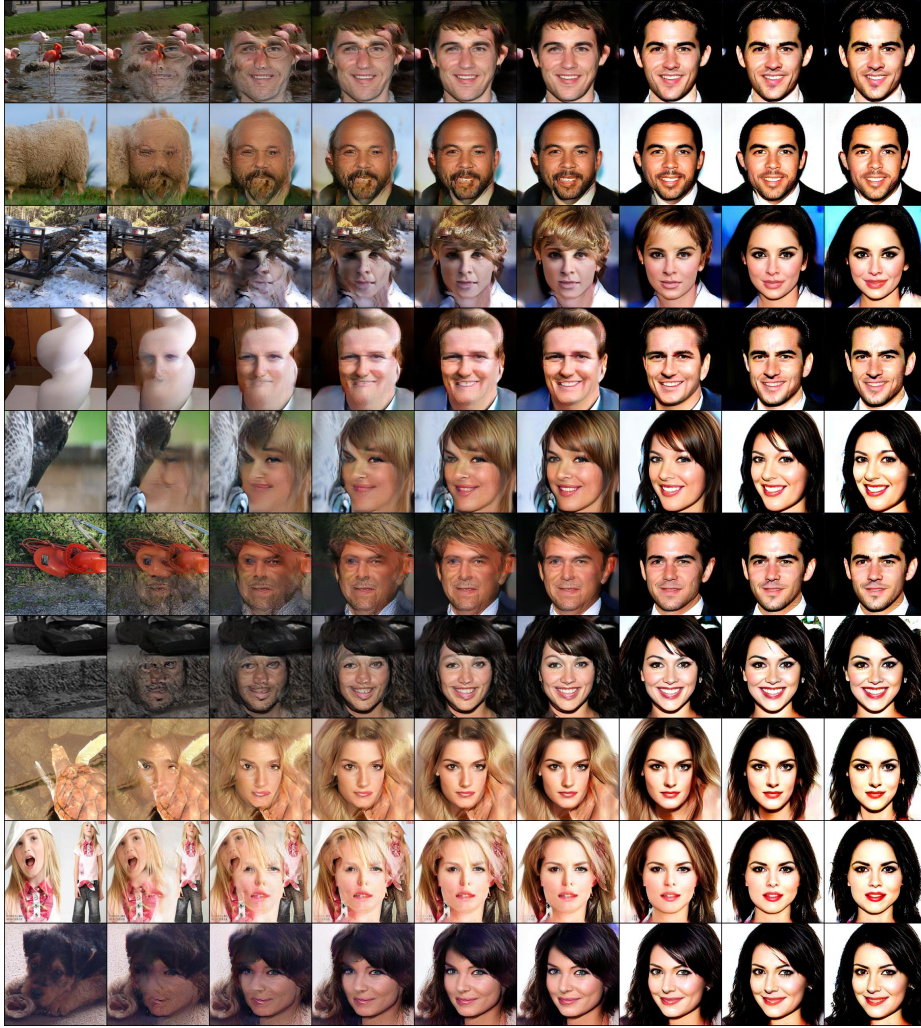


**Fig. 14.** CelebA-HQ 256 intermediate generation results. The PGD attack steps for column 1-9 are [ 0, 4, 8, 12, 16, 20, 30, 40, 50] (steps 20 has the best FID score).



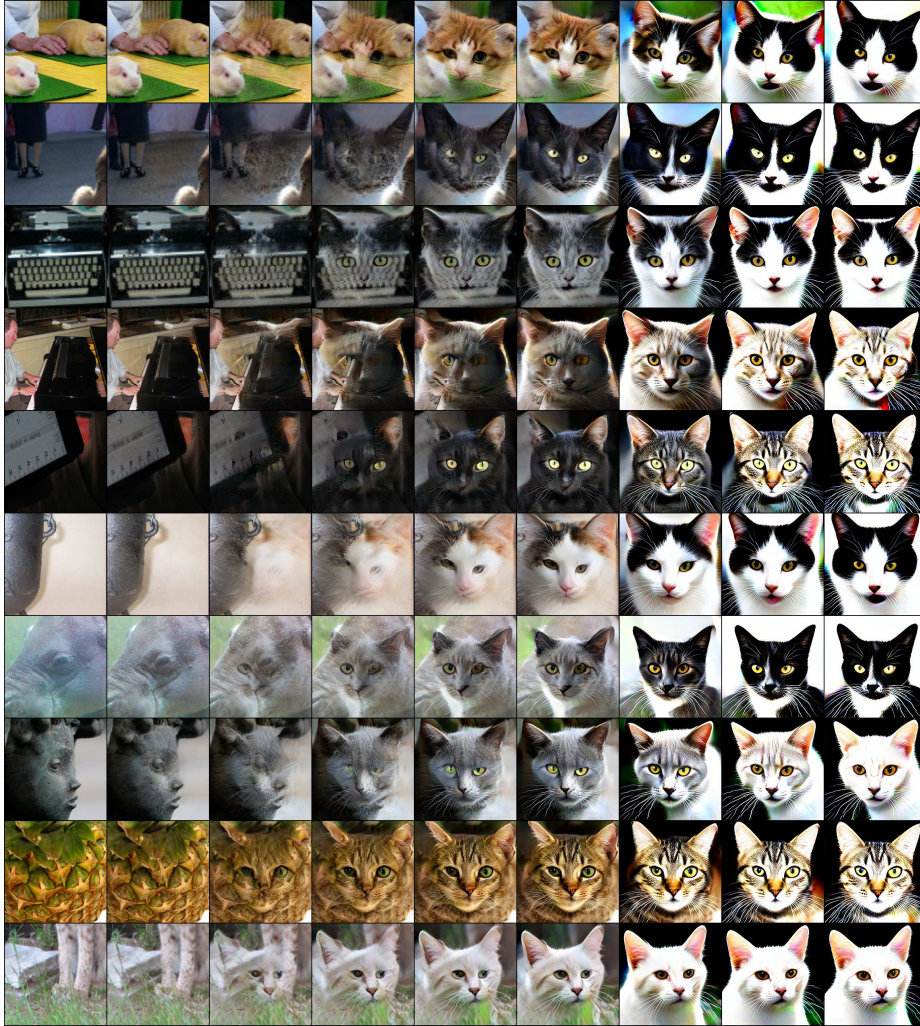


**Fig. 15.** AFHQ-CAT 256 intermediate generation results. The PGD attack steps for column 1-9 are [0, 2, 5, 8, 11, 14, 30, 50, 100] (steps 14 has the best FID score).

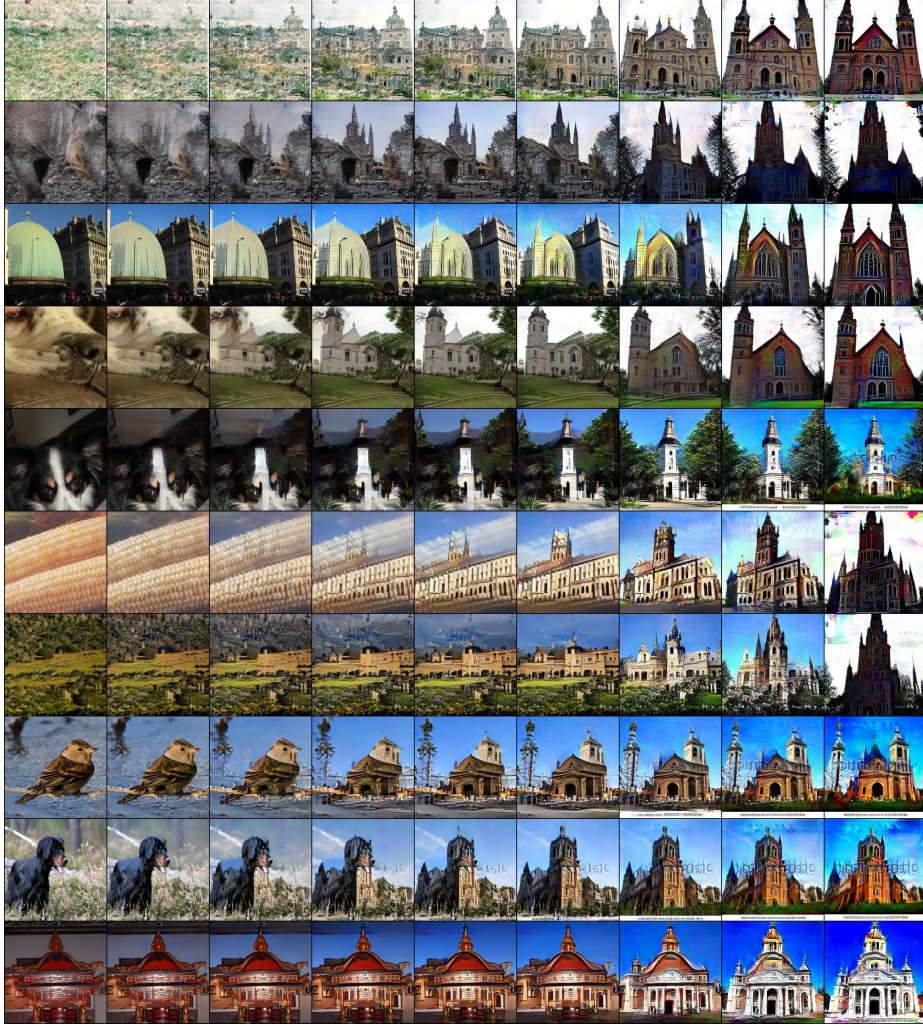


**Fig. 16.** LSUN-Church 256 intermediate generation results. The PGD attack steps for column 1-9 are [ 0, 3, 6, 10, 13, 17, 30, 50, 100] (steps 17 has the best FID score).

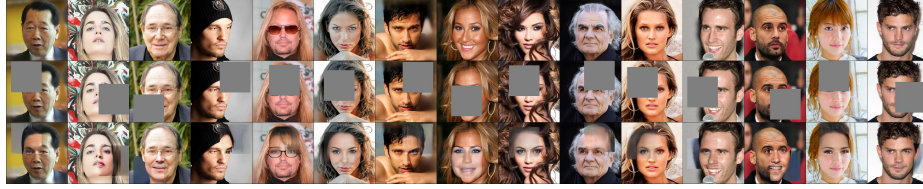




**Fig. 17.** Concept conjunction [10] using the CelebA-HQ model and AFHQ-CAT model. The generated samples have both human face features and cat face features.



Original images (1st row), images with additive Gaussian noise of standard deviation of 0.1 (2nd row), and recovered images (last row).



Original image (1st row), occluded images (2nd row), and recovered images (last row).

**Fig. 18.** Uncurated denoising and inpainting results on CelebA-HQ 256.



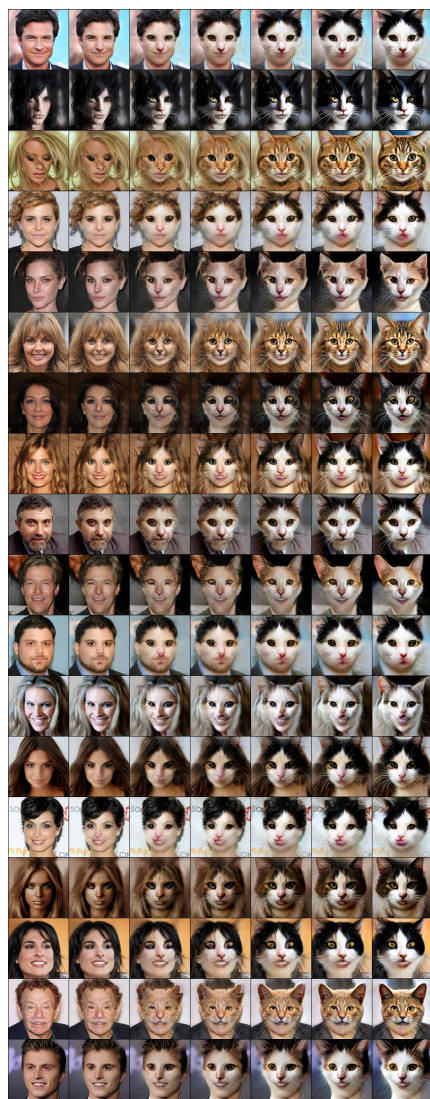
Original images (1st row), images with additive Gaussian noise of standard deviation of 0.1 (2nd row), and recovered images (last row).



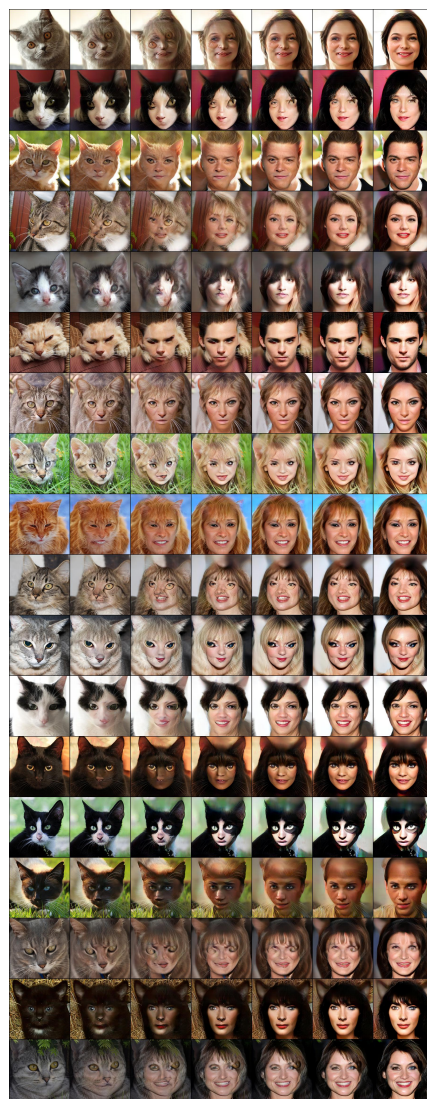
Original image (1st row), occluded images (2nd row), and recovered images (last row).

**Fig. 19.** Uncurated denoising and inpainting results on AFHQ-CAT 256.





Uncurated image translation results on  
CelebA-HQ 256.



Uncurated image translation results on  
AFHQ-CAT 256.

**Fig. 20.** Uncurated image translation samples.



**Fig. 21.** Seed images used to generate samples in Fig. 4, Fig. 5, Fig. 6, and Fig. 7.